Vertical Free Convective Boundary-Layer Flow in a Bidisperse Porous Medium

D. A. S. Rees
Department of Mechanical Engineering,
University of Bath,
Bath BA2 7AY, UK

D. A. Nield
Department of Engineering Science,
University of Auckland,
Private Bag 92019,
Auckland 1142, New Zealand

A. V. Kuznetsov
Department of Mechanical and Aerospace Engineering,
North Carolina State University,
Campus Box 7910,
Raleigh, NC 27695-7910

In this article, we study the effect of adopting a two-temperature and two-velocity model, appropriate to a bidisperse porous medium (BDPM), on the classical Cheng–Minkowycz study of vertical free convection boundary-layer flow in a porous medium. It is shown that the boundary-layer equations can be expressed in terms of three parameters: a modified volume fraction, a modified thermal conductivity ratio, and a third parameter incorporating both thermal and BDPM properties. A numerical simulation of the developing boundary layer is guided by a near-leading-edge analysis and supplemented by a far-field analysis. The study is completed by a presentation of numerical simulations of the elliptic equations in order to determine how the adoption of the BDPM model affects the thermal fields in the close vicinity of the origin. [DOI: 10.1115/1.2943304]

Keywords: bidisperse porous medium, free convection, numerical simulation, asymptotic analysis

1 Introduction

A bidisperse porous medium (BDPM, see Fig. 1), as informally defined by Chen et al. [1,2], is composed of clusters of large particles that are agglomerations of small particles. Thus, there are macropores between the clusters and micropores within them. Applications are found in bidisperse adsorbent or bidisperse capillary wicks in a heat pipe. Since the bidisperse wick structure significantly increases the area available for liquid film evaporation, it has been proposed for use in the evaporator of heat pipes.

A BDPM may thus be looked at as a standard porous medium in which the solid phase is replaced by another porous medium, whose temperature may be denoted by T_p if local thermal equilibrium (LTE) is assumed within each cluster. We can then talk about the f-phase (the macropores) and the p-phase (the remainder of the structure). An alternative way of looking at the structure is to regard it as a porous medium in which fractures or tunnels have been introduced. One can then think of the f-phase as being a "fracture phase" and the p-phase as being a "porous phase."

The Darcy model for the steady-state momentum transfer in a BDPM is represented by the following pair of coupled equations for the Darcy velocities $\mathbf{v}^*_f$ and $\mathbf{v}^*_p$, where the asterisks denote dimensional variables,

$$\mathbf{G} = \left(\frac{\mu}{K_f}\right)\mathbf{v}^*_f + \zeta(\mathbf{v}^*_f - \mathbf{v}^*_p) \tag{1a}$$

$$\mathbf{G} = \left(\frac{\mu}{K_p}\right)\mathbf{v}^*_p + \zeta(\mathbf{v}^*_p - \mathbf{v}^*_f) \tag{1b}$$

Here, $\mathbf{G}$ is the negative of the applied pressure gradient, μ is the fluid viscosity, K_f and K_p are the permeabilities of the two phases, and ζ is the coefficient for momentum transfer between the two phases.

These equations were applied by Nield and Kuznetsov [3,4] to forced convection in a channel and by Nield and Kuznetsov [5] to the Horton–Rogers–Lapwood problem (the paradigmatic problem for natural convection in an enclosed region). These studies were reviewed by Nield and Kuznetsov [6].

In this article, we apply the two-velocity two-temperature formulation to a problem that is paradigmatic for external natural convection in a porous medium, namely, the problem of convection past a vertical plate, a problem first considered by Cheng and Minkowycz [7]. The problem leads naturally to a boundary-layer formulation. We are guided by a study of Rees and Pop [8]. These authors used a model incorporating two temperatures (local thermal nonequilibrium (LTNE)) but a single velocity. Related work is presented in Mohamad [9], Rees and Pop [10], and Haddad et al. [11,12]. For the more general aspects of convection in a porous medium past a vertical plate, the reader is referred to the survey by Nield and Bejan [13]. A preliminary report on this topic was presented by Nield and Kuznetsov [14].

2 Analysis

We consider steady two-dimensional flow in a BDPM induced by a vertical heated plate held at the constant temperature T_w and embedded in the BDPM with ambient temperature T_∞. The equations of continuity (expressing conservation of mass) for the velocity components in the two phases are

$$\frac{\partial u^*_f}{\partial x^*} + \frac{\partial v^*_f}{\partial y^*} = 0 \tag{2a}$$

$$\frac{\partial u^*_p}{\partial x^*} + \frac{\partial v^*_p}{\partial y^*} = 0 \tag{2b}$$

We note that in the traditional Darcy formulation, the pressure is an intrinsic quantity, i.e., it is the pressure in the fluid. We recognize that in a BDPM, the fluid occupies all of the f-phase and a fraction of the p-phase. We denote the volume fraction of the f-phase by ϕ (something that in a regular porous medium would be called the porosity) and the porosity in the p-phase by ε. Thus, $1-\phi$ is the volume fraction of the p-phase, and the volume fraction of the BDPM occupied by the fluid is $\phi+(1-\phi)\varepsilon$. The volume average of the temperature over the fluid is

$$T_F^* = \frac{\phi T_f^* + (1-\phi)\varepsilon T_p^*}{\phi + (1-\phi)\varepsilon} \tag{3}$$

Contributed by the Heat Transfer Division of ASME for publication in the JOURNAL OF HEAT TRANSFER. Manuscript received June 14, 2007; final manuscript received October 24, 2007; published online July 11, 2008. Review conducted by Jamal Seyed-Yagoobi.

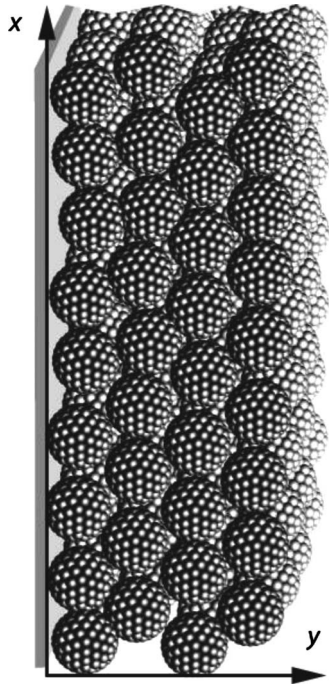

Fig. 1 Sketch of a BDPM adjacent to a vertical plate

The drag force (per unit volume) balances the gradient of the excess pressure over hydrostatic. Our basic hypothesis is that in a BDPM, the drag is increased by an amount $\zeta(\mathbf{v}_f^* - \mathbf{v}_p^*)$ for the f-phase and decreased by the same amount for the p-phase. Accordingly, we write the momentum equations as

$$\frac{\partial p^*}{\partial x^*} = -\frac{\mu}{K_f} u_f^* - \zeta(u_f^* - u_p^*) + \rho_F \hat{g}\hat{\beta}(T_F^* - T_\infty) \tag{4a}$$

$$\frac{\partial p^*}{\partial x^*} = -\frac{\mu}{K_p} u_p^* - \zeta(u_p^* - u_f^*) + \rho_F \hat{g}\hat{\beta}(T_F^* - T_\infty) \tag{4b}$$

$$\frac{\partial p^*}{\partial y^*} = -\frac{\mu}{K_f} v_f^* - \zeta(v_f^* - v_p^*) \tag{4c}$$

$$\frac{\partial p^*}{\partial y^*} = -\frac{\mu}{K_p} v_p^* - \zeta(v_p^* - v_f^*) \tag{4d}$$

Here, ρ_F is the density of the fluid, $\hat{\beta}$ is the volumetric thermal expansion coefficient of the fluid, and $\hat{g}$ is the gravitational acceleration. In writing Eqs. (4a) and (4b), we have recognized that variations of pressure due to buoyancy are intrinsic (rather than volume averaged) quantities, and so the usual procedure of averaging over a representative elementary volume is not necessarily appropriate. In the case of buoyancy, the solid and thermal conductivities are not involved, and so it is reasonable to treat the thermal aspect of buoyancy in a special way. It was found in Ref. [5] that a coherent mathematical representation required that the buoyancy terms in Eqs. (4a) and (4b) be the same.

The thermal energy equations are taken as

$$\phi(\rho c)_f \mathbf{v}_f^* \cdot \nabla T_f^* = \phi k_f \nabla^2 T_f^* + h(T_p^* - T_f^*) \tag{5a}$$

$$(1-\phi)(\rho c)_p \mathbf{v}_p^* \cdot \nabla T_p^* = (1-\phi) k_p \nabla^2 T_p^* + h(T_f^* - T_p^*) \tag{5b}$$

Here, c denotes the specific heat at constant pressure, k denotes the thermal conductivity, and h is an interphase heat transfer coefficient (incorporating the specific area). The precise definition of k_p is not important for our present purpose. It could be estimated by the weighted average, taken over the p-phase, of the fluid and solid conductivities.

It should be noted that since the velocity in the p-phase will generally be small in comparison to that in the macropores, it is a good approximation to assume thermal equilibrium within the p-phase. We assume homogeneity on the global scale. For further discussion on LTE, the reader is referred to Rees et al. [15].

We introduce dimensionless variables as follows:

$$(x^*, y^*) = d(\hat{x}, \hat{y}), \quad p^* = \frac{k_f \mu}{(\rho c)_f K_f} p \tag{6}$$

$$(u_f^*, v_f^*) = \frac{\phi k_f}{(\rho c)_f d}(\hat{u}_f, \hat{v}_f), \quad (u_p^*, v_p^*) = \frac{(1-\phi)k_p}{(\rho c)_p d}(\hat{u}_p, \hat{v}_p) \tag{7}$$

$$T_f^* = (T_w - T_\infty)\theta_f + T_\infty, \quad T_p^* = (T_w - T_\infty)\theta_p + T_\infty \tag{8}$$

We also introduce the stream functions $\hat{\psi}_f$ and $\hat{\psi}_p$ defined so that

$$\hat{u}_f = \frac{\partial \hat{\psi}_f}{\partial \hat{y}}, \quad \hat{v}_f = -\frac{\partial \hat{\psi}_f}{\partial \hat{x}}, \quad \hat{u}_p = \frac{\partial \hat{\psi}_p}{\partial \hat{y}}, \quad \hat{v}_p = -\frac{\partial \hat{\psi}_p}{\partial \hat{x}} \tag{9}$$

(We use the sign convention in Rees and Pop [8] rather than that in Nield and Kuznetsov [5].) We define a Rayleigh number R based on properties in the f-phase by

$$R = \frac{\rho_F \hat{g}\hat{\beta}(T_w - T_\infty) K_f d}{\mu \phi k_f / (\rho c)_f} \tag{10}$$

Elimination of the pressure from Eqs. (4a)–(4d) then leads to

$$(1+\sigma_f)\nabla^2 \hat{\psi}_f - \beta\sigma_f \nabla^2 \hat{\psi}_p = R\frac{\partial \theta_F}{\partial \hat{y}} \tag{11a}$$

$$-\sigma_f \nabla^2 \hat{\psi}_f + \beta\left(\frac{1}{K_r} + \sigma_f\right)\nabla^2 \hat{\psi}_p = R\frac{\partial \theta_F}{\partial \hat{y}} \tag{11b}$$

where

$$\frac{\partial \theta_F}{\partial \hat{y}} = \frac{\varphi \dfrac{\partial \theta_f}{\partial \hat{y}} + (1-\phi)\varepsilon \dfrac{\partial \theta_p}{\partial \hat{y}}}{\phi + (1-\phi)\varepsilon} \tag{12}$$

Here, we have introduced the dimensionless parameters

$$\sigma_f = \frac{\zeta K_f}{\mu}, \quad \beta = \frac{(1-\phi)k_p(\rho c)_f}{\phi k_f (\rho c)_p} \tag{13}$$

Thus, σ_f is an interphase momentum transfer parameter, while β is a modified thermal diffusivity ratio. Also, the thermal energy equations ((5a) and (5b)) become

$$\nabla^2 \theta_f = \hat{h}(\theta_f - \theta_p) + \frac{\partial \hat{\psi}_f}{\partial \hat{y}}\frac{\partial \theta_f}{\partial \hat{x}} - \frac{\partial \hat{\psi}_f}{\partial \hat{x}}\frac{\partial \theta_f}{\partial \hat{y}} \tag{14a}$$

$$\nabla^2 \theta_p = \gamma\hat{h}(\theta_p - \theta_f) + \frac{\partial \hat{\psi}_p}{\partial \hat{y}}\frac{\partial \theta_p}{\partial \hat{x}} - \frac{\partial \hat{\psi}_p}{\partial \hat{x}}\frac{\partial \theta_p}{\partial \hat{y}} \tag{14b}$$

where

$$\gamma = \frac{\phi k_f}{(1-\phi)k_p}, \quad \hat{h} = \frac{hd^2}{\phi k_f} \tag{15}$$

Thus, γ is a modified thermal conductivity ratio and $\hat{h}$ is an interphase heat transfer parameter.

Next, we introduce the boundary-layer scaling,

$$\hat{x} = x, \quad \hat{y} = R^{-1/2} y, \quad \hat{\psi}_f = R^{1/2}\psi_f, \quad \hat{\psi}_p = R^{1/2}\psi_p \tag{16}$$

and the shorthand notation

$$\tau = \frac{\phi}{\phi + (1-\phi)\varepsilon}, \quad K_r = \frac{K_p}{K_f} \tag{17}$$

Then, we get

$$(1+\sigma_f)\frac{\partial^2 \hat{\psi}_f}{\partial y^2} - \beta\sigma_f \frac{\partial^2 \hat{\psi}_p}{\partial y^2} = \tau\frac{\partial \theta_f}{\partial y} + (1-\tau)\frac{\partial \theta_p}{\partial y} \tag{18a}$$

$$-\sigma_f \frac{\partial^2 \hat{\psi}_f}{\partial y^2} + \beta\left(\frac{1}{K_r} + \sigma_f\right)\frac{\partial^2 \hat{\psi}_p}{\partial y^2} = \tau\frac{\partial \theta_f}{\partial y} + (1-\tau)\frac{\partial \theta_p}{\partial y} \tag{18b}$$

$$\frac{\partial^2 \theta_f}{\partial y^2} = H(\theta_f - \theta_p) + \frac{\partial \psi_f}{\partial y}\frac{\partial \theta_f}{\partial x} - \frac{\partial \psi_f}{\partial x}\frac{\partial \theta_f}{\partial y} \tag{18c}$$

$$\frac{\partial^2 \theta_p}{\partial y^2} = \gamma H(\theta_p - \theta_f) + \frac{\partial \psi_p}{\partial y}\frac{\partial \theta_p}{\partial x} - \frac{\partial \psi_p}{\partial x}\frac{\partial \theta_p}{\partial y} \tag{18d}$$

where

$$H = \hat{h}/R \tag{19}$$

The appropriate boundary conditions are

$$\psi_f = 0, \quad \psi_p = 0, \quad \theta_f = 1, \quad \theta_p = 1 \quad \text{at } y = 0 \tag{20a}$$

$$\frac{\partial \psi_f}{\partial y}, \ \frac{\partial \psi_p}{\partial y}, \ \theta_f, \theta_p \to 0 \quad \text{as } y \to \infty \tag{20b}$$

These boundary conditions allow Eqs. (18*a*) and (18*b*) to be integrated once to yield

$$(1+\sigma_f)\frac{\partial \hat{\psi}_f}{\partial y} - \beta\sigma_f \frac{\partial \hat{\psi}_p}{\partial y} = \tau\theta_f + (1-\tau)\theta_p \tag{21a}$$

$$-\sigma_f \frac{\partial \hat{\psi}_f}{\partial y} + \beta\left(\frac{1}{K_r} + \sigma_f\right)\frac{\partial \hat{\psi}_p}{\partial y} = \tau\theta_f + (1-\tau)\theta_p \tag{21b}$$

We now introduce the usual boundary-layer transformation appropriate to the Cheng–Minkowycz problem:

$$\psi_f = x^{1/2} f(x,\eta), \quad \psi_p = x^{1/2} g(x,\eta) \tag{22a}$$

$$\theta_f = \theta_f(x,\eta), \quad \theta_p = \theta_p(x,\eta) \tag{22b}$$

where

$$\eta = \frac{y}{x^{1/2}} \tag{23}$$

One then has the system

$$(1+\sigma_f)f' - \beta\sigma_f g' = \tau\theta_f + (1-\tau)\theta_p \tag{24a}$$

$$-\sigma_f f' + \beta\left(\frac{1}{K_r} + \sigma_f\right)g' = \tau\theta_f + (1-\tau)\theta_p \tag{24b}$$

$$\theta_f'' + \tfrac{1}{2} f\theta_f' = Hx(\theta_f - \theta_p) + x(f'\theta_{fx} - \theta_f' f_x) \tag{24c}$$

$$\theta_p'' + \tfrac{1}{2} g\theta_p' = \gamma Hx(\theta_p - \theta_f) + x(g'\theta_{px} - \theta_p' g_x) \tag{24d}$$

subject to the boundary conditions

$$f = 0, \quad g = 0, \quad \theta_f = 1, \quad \theta_p = 1 \quad \text{at } \eta = 0 \tag{24e}$$

$$\theta_f, \theta_p \to 0 \quad \text{as } \eta \to \infty \tag{24f}$$

It is worth noting that the boundary conditions (24*f*), together with Eqs. (24*a*) and (24*b*), imply that $f', g' \to 0$ as $\eta \to \infty$. In these equations, the primes denote derivatives with respect to η and the x-subscripts denote derivatives with respect to x.

Equations (24*a*)–(24*d*) contain six parameters. Before we proceed further, we demonstrate that the number of parameters can be reduced to 3. The transformation

$$f(\eta) = C_f F(\eta) \tag{25a}$$

$$g(\eta) = C_p G(\eta) \tag{25b}$$

where

$$C_f = \frac{1 + 2K_r\sigma_f}{1 + \sigma_f + K_r\sigma_f} = \frac{\mu + 2\zeta K_p}{\mu + \zeta K_f + \zeta K_p} \tag{26a}$$

$$C_p = \frac{K_r + 2K_r\sigma_f}{\beta(1 + \sigma_f + K_r\sigma_f)} = \frac{\phi}{1-\phi}\left(\frac{K_p}{K_f}\right)\left(\frac{k_f/(\rho c)_f}{k_p/(\rho c)_p}\right)C_f \tag{26b}$$

reduces Eqs. (24*a*), (24*b*), and (24*e*) to the form

$$F' = \tau\theta_f + (1-\tau)\theta_p \tag{27a}$$

$$G' = \tau\theta_f + (1-\tau)\theta_p \tag{27b}$$

$$F = 0, \quad G = 0, \quad \theta_f = 1, \quad \theta_p = 1 \quad \text{at } \eta = 0 \tag{27c}$$

From Eqs. (27*a*) and (27*b*), $F-G$ has zero derivative everywhere, and by Eq. (27*c*) has zero value at $\eta=0$, and so $F-G$ is identically zero; that is, $F \equiv G$. Using this fact, Eqs. (24*c*) and (24*d*) then reduce to

$$\theta_f'' + \frac{C_f}{2} F\theta_f' = Hx(\theta_f - \theta_p) + C_f x(F'\theta_{fx} - \theta_f' F_x) \tag{27d}$$

$$\theta_p'' + \frac{C_p}{2} F\theta_p' = \gamma Hx(\theta_p - \theta_f) + C_p x(F'\theta_{px} - \theta_p' F_x) \tag{27e}$$

We now introduce

$$A = (C_f^{\,2} + C_p^{\,2})^{1/2} \tag{28a}$$

$$\delta = \tan^{-1}(C_p/C_f) = \tan^{-1}\left(\frac{\phi}{1-\phi}\left(\frac{K_p}{K_f}\right)\left(\frac{k_f/(\rho c)_f}{k_p/(\rho c)_p}\right)\right) \tag{28b}$$

so that

$$C_f = A\cos\delta \tag{28c}$$

$$C_p = A\sin\delta \tag{28d}$$

and rescale so that

$$F(\eta) = \tilde{F}(\tilde{\eta})/A \tag{29a}$$

$$\eta = \tilde{\eta}/A \tag{29b}$$

At the same time, one can then eliminate the parameter H by using the transformation

$$\xi = Hx \tag{30}$$

to get the set of differential equations

$$\tilde{F}' = \tau\theta_f + (1-\tau)\theta_p \tag{31a}$$

$$\theta_f'' + \frac{\cos\delta}{2}\tilde{F}\theta_f' = \xi(\theta_f - \theta_p) + \cos\delta\,\xi(\tilde{F}'\theta_{f\xi} - \theta_f'\tilde{F}_\xi) \tag{31b}$$

$$\theta_p'' + \frac{\sin\delta}{2}\tilde{F}\theta_p' = \gamma\xi(\theta_p - \theta_f) + \sin\delta\,\xi(\tilde{F}'\theta_{p\xi} - \theta_p'\tilde{F}_\xi) \tag{31c}$$

The primes now denote derivatives with respect to $\tilde{\eta}$. These differential equations are subject to the boundary conditions,

$$\tilde{F} = 0, \quad \theta_f = 1, \quad \theta_p = 1 \quad \text{at } \xi = 0 \tag{31d}$$

$$\theta_f, \theta_p \to 0 \quad \text{as } \xi \to \infty \tag{31e}$$

We observe that we now have just three parameters, τ, γ, and δ, as defined by Eqs. (17), (15), and (28*b*), respectively, representing a volume fraction, a modified thermal conductivity ratio, and a

combination of thermal and BDPM parameters. The dependent variables are a single stream function and two temperatures.

3 Analysis Near the Leading Edge

We now perform an expansion in powers of ξ to third order starting from equations Eq. (31*a*)–(31*c*). Accordingly, we make the expansion

$$(\tilde{F},\theta_f,\theta_p)=(\tilde{F}_0,\theta_{f0},\theta_{p0})+\xi(\tilde{F}_1,\theta_{f1},\theta_{p1})+\xi^2(\tilde{F}_2,\theta_{f2},\theta_{p2})+\xi^3(\tilde{F}_3,\theta_{f3},\theta_{p3})+\ldots \tag{32}$$

and obtain the equations

$$\tilde{F}_n{}'=\tau\theta_{fn}+(1-\tau)\theta_{pn}\quad \text{for } n=0,1,2,3 \tag{33a}$$

$$\theta_{f0}''+\frac{\cos\delta}{2}\tilde{F}_0\theta_{f0}'=0 \tag{33b}$$

$$\theta_{f1}''+\frac{\cos\delta}{2}(\tilde{F}_0\theta_{f1}'+\tilde{F}_1\theta_{f0}')=\theta_{f0}-\theta_{p0}+\cos\delta[\tilde{F}_0'\theta_{f1}-\theta_{f0}'\tilde{F}_1] \tag{33c}$$

$$\theta_{f2}''+\frac{\cos\delta}{2}(\tilde{F}_0\theta_{f2}'+\tilde{F}_1\theta_{f1}'+\tilde{F}_2\theta_{f0}')=\theta_{f1}-\theta_{p1}+\cos\delta[2(\tilde{F}_0'\theta_{f2}-\theta_{f0}'\tilde{F}_2)+(\tilde{F}_1'\theta_{f1}-\theta_{f1}'\tilde{F}_1)] \tag{33d}$$

$$\theta_{f3}''+\frac{\cos\delta}{2}(\tilde{F}_0\theta_{f3}'+\tilde{F}_1\theta_{f2}'+\tilde{F}_2\theta_{f1}'+\tilde{F}_3\theta_{f0}')=\theta_{f2}-\theta_{p2}+\cos\delta[3(\tilde{F}_0'\theta_{f3}-\theta_{f0}'\tilde{F}_3)+2(\tilde{F}_1'\theta_{f2}-\theta_{f1}'\tilde{F}_2)+(\tilde{F}_2'\theta_{f1}-\theta_{f2}'\tilde{F}_1)] \tag{33e}$$

together with similar equations for θ_p.

In particular, the zero-order system is

$$\tilde{F}'=\tau\theta_{f0}+(1-\tau)\theta_{p0} \tag{34a}$$

$$\theta_{f0}''+\frac{\cos\delta}{2}\tilde{F}\theta_{f0}'=0 \tag{34b}$$

$$\theta_{p0}''+\frac{\sin\delta}{2}\tilde{F}\theta_{p0}'=0 \tag{34c}$$

$$\tilde{F}=0,\quad \theta_{f0}=1,\quad \theta_{p0}=1\quad \text{at } x=0 \tag{34d}$$

$$\theta_{f0},\theta_{p0}\to 0\quad \text{as } x\to\infty \tag{34e}$$

For the regular (monodisperse) porous medium (the case $\sigma_f=0$, $K_r=0$, $\tau=1$, that is, for $\delta=0$, $\tau=1$) the system of equations reduces to

$$f_0'=\theta_0 \tag{35a}$$

$$\theta_{f0}''+\tfrac{1}{2}f_0\theta_{f0}'=0 \tag{35b}$$

$$\theta_{f0}=1 \tag{35c}$$

the solution of which was presented by Cheng and Minkowycz [7]. The chief features of interest are that

$$f_0\to 1.61613\quad \text{as } \eta\to\infty \tag{36a}$$

$$\theta_0'(0)=-0.44378 \tag{36b}$$

and θ_0 becomes exponentially small as $\eta\to\infty$. The numerical values are those obtained by Rees and Pop [8].

4 Analysis Far From the Leading Edge

We consider the situation when x (and therefore ξ) is asymptotically large. We expand $\tilde{F}$, θ_f, and θ_p in the form

$$(\tilde{F},\theta_f,\theta_p)=(\tilde{F}^{(0)},\theta_f^{(0)},\theta_p^{(0)})+\xi^{-1}(\tilde{F}^{(1)},\theta_f^{(1)},\theta_p^{(1)})+\ldots \tag{37}$$

Substitution into Eqs. (31*a*)–(31*c*) gives at leading order

$$\theta_f^{(0)}-\theta_p^{(0)}=0 \tag{38}$$

and hence $\theta_f^{(0)}=\theta_p^{(0)}\equiv\theta^{(0)}$, say.

Using this result, at the next order, one has

$$F_\eta^{(0)}=\theta^{(0)} \tag{39a}$$

$$\theta_{\eta\eta}^{(0)}+\frac{\cos\delta}{2}\tilde{F}^{(0)}\theta_\eta^{(0)}=\theta_f^{(1)}-\theta_p^{(1)} \tag{39b}$$

$$\theta_{\eta\eta}^{(0)}+\frac{\sin\delta}{2}\tilde{F}^{(0)}\theta_\eta^{(0)}=\gamma(\theta_p^{(1)}-\theta_f^{(1)}) \tag{39c}$$

A linear combination of the last two equations then gives

$$\theta_{\eta\eta}^{(0)}+\frac{\Gamma}{2}\tilde{F}^{(0)}\theta_\eta^{(0)}=0 \tag{39d}$$

where

$$\Gamma=\frac{\gamma\cos\delta+\sin\delta}{\gamma+1} \tag{40}$$

Then the transformation

$$\tilde{\zeta}=\Gamma^{1/2}\eta,\quad \hat{F}^{(0)}(\tilde{\zeta})=\Gamma^{1/2}\tilde{F}^{(0)}(\eta) \tag{41}$$

gives

$$\hat{F}_{\tilde{\zeta}}^{(0)}=\theta^{(0)} \tag{42a}$$

$$\theta_{\tilde{\zeta}\tilde{\zeta}}^{(0)}+\frac{1}{2}\hat{F}^{(0)}\theta_{\tilde{\zeta}}^{(0)}=0 \tag{42b}$$

The boundary conditions for this set of differential equations are

$$\hat{F}^{(0)}=0,\quad \theta^{(0)}=1\quad \text{at } \tilde{\zeta}=0 \tag{42c}$$

$$\theta^{(0)}\to 0\quad \text{as } \tilde{\zeta}\to\infty \tag{42d}$$

Thus, again, we have the system studied by Cheng and Minkowycz [7].

At the next order of asymptotic approximation, one has a homogenous linear system of differential equations and boundary conditions for $\theta_f^{(1)}$ and $\theta_p^{(1)}$, which admits an eigensolution of arbitrary magnitude. This means that we have an insoluble system of equations at $O(\xi^{-1})$. One could, in principle, proceed further by introducing $\xi^{-1}\ln\xi$ terms, as was done by Rees and Pop [8], but we judged that in the present case there would be little gain in doing so since the $\xi^{-1}\ln\xi$ and ξ^{-1} terms can only be differentiated in terms of their magnitude at exceptionally large values of ξ.

5 Numerical Solutions

Three different numerical schemes were used to obtain the results displayed in Figs. 2–6. First, a standard fourth order Runge–Kutta scheme was used together with a multiple shooting strategy to solve the small-ξ equations given in Eqs. (34*a*)–(34*e*). We found that $\eta_{\max}=10$ is sufficient to contain the boundary layer for the leading order terms, F_0, θ_{f0}, and θ_{p0}. However, when four terms are taken, it is essential to take $\eta_{\max}$ to be at least 25, although $\eta_{\max}=40$ was used with 400 uniformly spaced intervals. We define Q_f and Q_p to be the derivatives of the temperature fields at the surface:

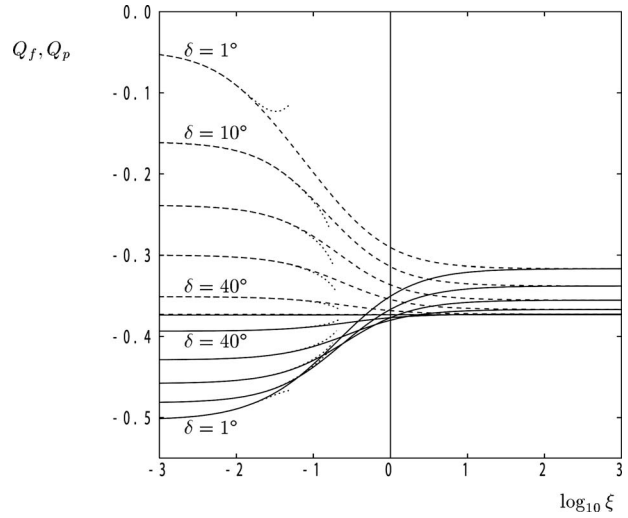

Fig. 2 Variation of Q_f (continuous lines) and Q_p (long dashes) with ξ for τ=0.5 and γ=1, where δ takes the values of 1 deg, 10 deg, 20 deg, 30 deg, 40 deg, and 44.9 deg. Also shown are the four-term small-ξ expansions (dotted lines).

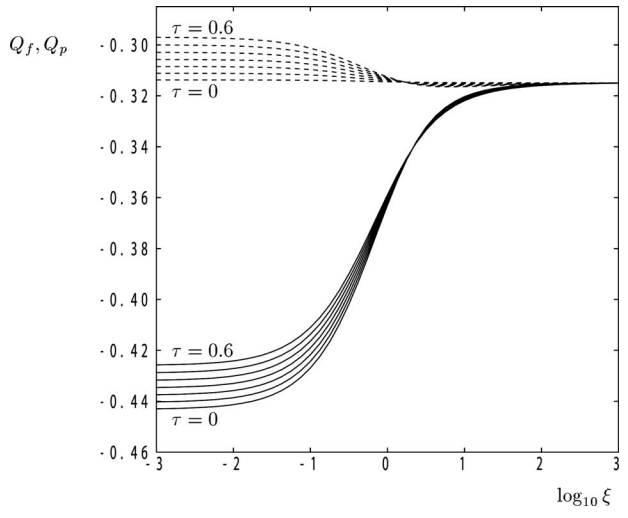

Fig. 4 Variation of Q_f (continuous lines) and Q_p (long dashes) with ξ for $\gamma=10^{-2}$ and δ=30 deg, where τ takes the values of 0.0, 0.1, 0.2, 0.3, 0.4, 0.5, and 0.6

$$Q_f = \left.\frac{\partial\theta_f}{\partial\eta}\right|_{\eta=0} \quad \text{and} \quad Q_p = \left.\frac{\partial\theta_p}{\partial\eta}\right|_{\eta=0} \tag{43}$$

and these are plotted in Figs. 2–4.

Second, the parabolic system of equations given by Eqs. (31*a*)–(31*c*) was solved using the Keller-box method. The governing equations were rewritten in first order form in η, discretized using central differences in both η and ξ, and the resulting nonlinear difference equations were solved using a multidimensional Newton–Raphson scheme. The details of the block-Thomas algorithm, which is used for this purpose is now quite standard. For these simulations, we used $\eta_{\max}=25$ with 500 uniformly spaced intervals. Although this method is formally of second order accuracy, the solutions obtained at $\xi=0$ are precisely the same as those obtained for F_0, θ_{f0}, and θ_{p0} to four significant figures. We used a nonuniform grid in the ξ-direction, which was formed by using a uniform grid in $\log_{10}\xi$ for all points except for at $\xi=0$.

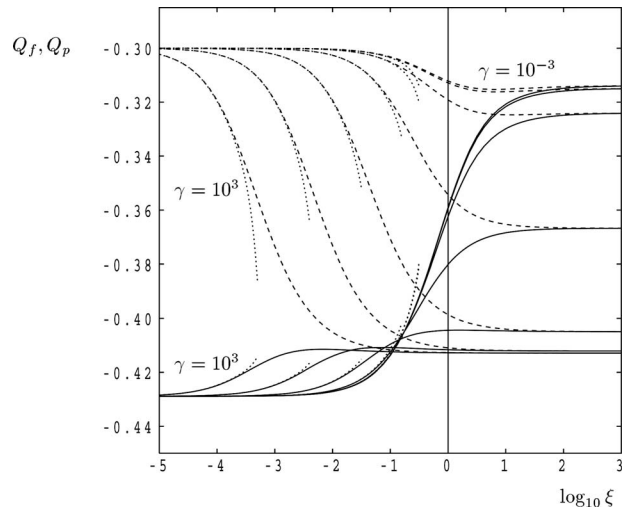

Fig. 3 Variation of Q_f (continuous lines) and Q_p (long dashes) with ξ for τ=0.5 and δ=30 deg, where γ takes the values of 10^{-2}, 10^{-1}, 1, 10, 10^2, and 10^3. Also shown are the four-term small-ξ expansions (dotted lines).

Third, the full elliptic system given by Eqs. (11*a*), (11*b*), (14*a*), and (14*b*) was solved using an implicit time-stepping code. Rees and Bassom [16] considered the flow induced by a uniformly hot semi-infinite surface bounding an otherwise cold monodisperse porous medium subject to LTE, and found that the full steady elliptic equations reduce to ordinary differential form when written in parabolic coordinates, and when the porous medium is taken to occupy the semi-infinite region $y \geq 0$. Thus, parabolic coordinates offer a computationally efficient means for solving the governing equations for complicated cases, such as the stability analysis of Rees [17] and the study of LTNE effects by Rees [18]. In both these cases, time stepping was undertaken using a backward difference in time with second order central differences in space. The fully implicit scheme also employed coordinate stretching to increase the efficiency of the code, and the solution at each time step was obtained using the full multigrid methodology with V-cycling; further details may be found in Rees [17].

The parabolic coordinate system we used is given by the transformation

$$X = (\bar{\xi}^2 - \bar{\eta}^2)/4, \quad Y = \bar{\xi}\bar{\eta}/2 \tag{44}$$

following the transformation of Eq. (18) by

$$\Psi = R^{1/2}\psi, \quad X = R^{-1/2}x, \quad Y = R^{-1/2}y \tag{45}$$

to obtain

$$\frac{\partial^2\Psi}{\partial\bar{\xi}^2} + \frac{\partial^2\Psi}{\partial\bar{\eta}^2} = \tau\left[\frac{\bar{\xi}}{2}\frac{\partial\theta_f}{\partial\bar{\eta}} + \frac{\bar{\eta}}{2}\frac{\partial\theta_f}{\partial\bar{\xi}}\right] + (1-\tau)\left[\frac{\bar{\xi}}{2}\frac{\partial\theta_p}{\partial\bar{\eta}} + \frac{\bar{\eta}}{2}\frac{\partial\theta_p}{\partial\bar{\xi}}\right] \tag{46a}$$

$$\frac{(\bar{\xi}^2+\bar{\eta}^2)}{4}\left[\frac{\partial\theta_f}{\partial t} + H\cos\delta(\theta_f - \theta_p)\right] = \frac{\partial^2\theta_f}{\partial\bar{\xi}^2} + \frac{\partial^2\theta_f}{\partial\bar{\eta}^2} + \cos\delta\left[\frac{\partial\Psi}{\partial\bar{\xi}}\frac{\partial\theta_f}{\partial\bar{\eta}} - \frac{\partial\Psi}{\partial\bar{\eta}}\frac{\partial\theta_f}{\partial\bar{\xi}}\right] \tag{46b}$$

$$\frac{(\bar{\xi}^2+\bar{\eta}^2)}{4}\left[\frac{\partial\theta_p}{\partial t} + H\gamma\sin\delta(\theta_p - \theta_f)\right] = \frac{\partial^2\theta_p}{\partial\bar{\xi}^2} + \frac{\partial^2\theta_p}{\partial\bar{\eta}^2} + \sin\delta\left[\frac{\partial\Psi}{\partial\bar{\xi}}\frac{\partial\theta_p}{\partial\bar{\eta}} - \frac{\partial\Psi}{\partial\bar{\eta}}\frac{\partial\theta_p}{\partial\bar{\xi}}\right] \tag{46c}$$

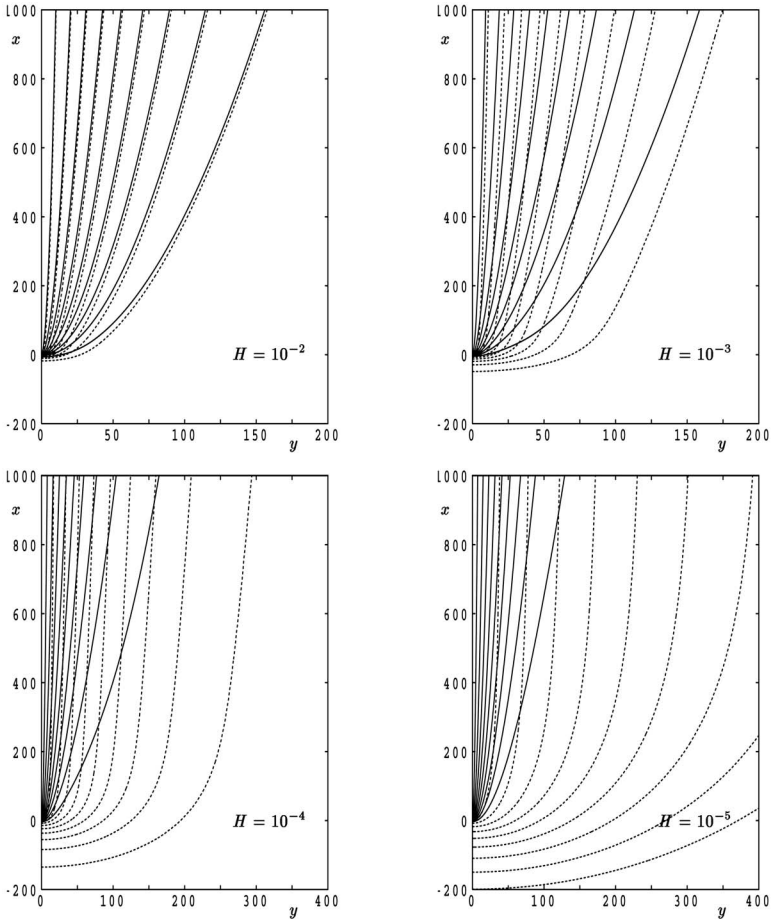

Fig. 5 Isotherms for both the fluid phase (continuous lines) and solid phase (dashed lines) for γ=1.0, τ=1, δ=0 for various values of *H*

We note that when x is large (and therefore $\bar{\xi}$ is large), the coordinate $\bar{\eta}$ is almost identical to the boundary-layer coordinate, η. In our simulations, we also employed an exponential coordinate stretching in both the $\bar{\xi}$ and $\bar{\eta}$ directions. In particular, we took $\bar{\eta}=e^{\hat{\eta}}-1$, where $\hat{\eta}_{\max}$ was taken to be 3.5. This means that $\bar{\eta}_{\max} \approx 31.16$, which is in excess of the value, 25, which we deemed earlier to be the minimum that could be used. We employed 128 grid points in the $\bar{\xi}$ direction and 64 in the $\bar{\eta}$ direction.

6 Results and Discussion

Figures 2–4 show how the surface rates of heat transfer, Q_f and Q_p, vary with ξ for various combinations of the governing parameters, γ, δ, and τ. These figures show the results of the parabolic simulations, while comparisons to the four-term small-ξ expansion are shown in Figs. 2 and 3 only.

Figure 2 concentrates on the values $\tau=0.5$ and $\gamma=1$ and depicts how the heat transfer characteristics change with the value of δ, where we note (i) that $\delta=0$ corresponds to a monodisperse system where the p-phase is solid (and therefore we should also have $\tau=1$) and (ii) that $\delta=45$ deg corresponds to a situation where the two phases act identically.

In all cases (except for $\delta=45$ deg), the porous medium is subject to strong LTNE between the phases near the leading edge. The mathematical reason for this is that the boundary layer equations for the respective phases are decoupled at leading order, while the physical reason is the asymmetry between the phases, in general, where advection is much stronger in the fluid phase. As ξ increases, the source/sink terms become more effective and this results in the gradual approach to LTE. The detailed numerical results show that LTE is established later as δ reduces toward zero; this is because of the decreasing amount of advection in the p-phase in that limit.

The effect of varying γ is shown in Fig. 3 for the case where $\tau=0.5$ and $\delta=30$ deg. Here, we have taken γ in the range from 10^{-3} to 10^{3}. Given that γ multiplies the source/sink terms in the θ_p equation, it is not a surprise to see that LTE is established very early (i.e., at small values of ξ) when γ is large, but is delayed considerably when γ is small. We can also see that the range of validity of the small-ξ expansion depends very strongly on the value of γ, unlike the situation shown in Fig. 2.

When τ is allowed to vary, we are allowing the relative magnitudes of the buoyancy forces corresponding to the two phases to change. When $\gamma=10^{-2}$ and $\delta=30$ deg, the curves shown in Fig. 4 indicate that there is a little change in the detailed evolution of the rate of heat transfer with ξ. This is not unexpected, because τ is a volume fraction independent of any thermal property. At any chosen value of ξ, the corresponding set of curves for larger values of γ are found to vary even less than those shown in Fig. 4.

Table 1 shows how the large-ξ asymptotic analysis given in Sec. 5 compares to the parabolic simulations at $\xi=10^{5}$ for one typical parameter set. This table shows that the leading order solutions are reproduced exceptionally well by the parabolic simulations.

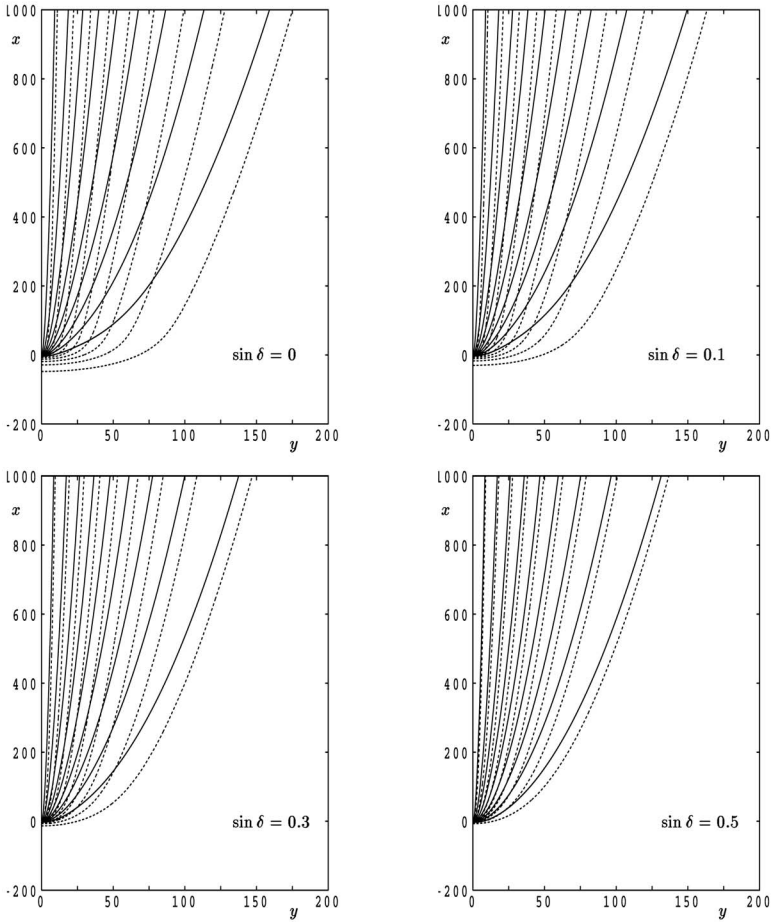

Fig. 6 Isotherms for both the fluid phase (continuous lines) and solid phase (dashed lines) for γ=1.0, τ=0.8, H=0.001 for various values of δ

The above discussion centered on situations where the boundary-layer approximation is valid, and therefore streamwise diffusion has been neglected. Thus, the small-ξ analysis is, strictly speaking, valid only while the boundary-layer approximation remains valid. We therefore turn our attention to the detailed convection, which takes place near to the leading edge of the heated surface. Figures 5 and 6 depict the isotherms for both phases for a variety of cases within this elliptic regime.

Figure 5 shows how the magnitude of H affects the thermal fields when γ=1, τ=1, and δ=0 deg. For relatively large values of H, which, in the present context means values that are greater than 0.01, the two phases are almost in LTE even in the region near the leading edge. However, as H decreases, the p-phase is affected decreasingly by the fluid movement in the f-phase, and therefore the temperature field in the p-phase is able to conduct with decreasing hindrance. Conversely, as the f-phase is increasingly isolated from the p-phase, the thickness of its boundary layer decreases as H decreases.

Figure 6 indicates how variations in δ affect the thermal fields when H=0.001, γ=1, and τ=0.8. When δ=0, we recover a situation with fairly strong LTNE because H is fairly small. However, the fact that γ=1 means that, once again, the phases satisfy identical energy equations when δ=45 deg and they will then be in global LTE. This figure shows the approach to LTE as δ varies from zero toward 45 deg.

Finally, we mention that variations in τ yield almost no discernable change in the isotherms; this is in accord with Fig. 4.

Table 1 Comparison of the large-ξ asymptotic solutions [see Eqs. (41), (42*a*), and (42*b*)] with the values obtained using the parabolic solver at ξ=10^5 (with δ=30 deg and τ=0.5). At least four significant figures of accuracy are attained.

γ	$f(\infty)$	$\theta'(0)$	$1.61613/\Gamma^{1/2}$	$-0.44378\Gamma^{1/2}$
0.001	2.284701	−0.313899	2.28472	−0.31391
0.01	2.277300	−0.314920	2.27731	−0.31494
0.1	2.213098	−0.324057	2.21310	−0.32407
1	1.955555	−0.366739	1.95552	−0.36676
10	1.771048	−0.404950	1.77100	−0.40497
100	1.740335	−0.412096	1.74029	−0.41212
1000	1.737057	−0.412874	1.73701	−0.41290

7 Concluding Remarks

If one wishes to generalize the interphase coupling in the BDPM model by replacing Eqs. (1*a*) and (1*b*) by

$$\mathbf{G} = \left(\frac{\mu}{K_f}\right)\mathbf{v}^*_f + \zeta(\mathbf{v}^*_f - b\mathbf{v}^*_p) \tag{47a}$$

$$\mathbf{G} = \left(\frac{\mu}{K_p}\right)\mathbf{v}^*_p + \zeta(c\mathbf{v}^*_p - d\mathbf{v}^*_f) \tag{47b}$$

then our previous analysis carries through but now Eqs. (26*a*) and (26*b*) are replaced by

$$C_f = \frac{1 + (b + c)K_r\sigma_f}{1 + (1 + cK_r)\sigma_f + (c - bd)K_r\sigma_f^2} \tag{48a}$$

$$C_p = \frac{K_r + (1 + d)K_r\sigma_f}{\beta[1 + (1 + cK_r)\sigma_f + (c - bd)K_r\sigma_f^2]} \tag{48b}$$

As a consequence, one then has

$$\delta = \tan^{-1}\left\{\frac{K_r}{\beta}\left[\frac{1 + (1 + d)\sigma_f}{1 + (b + c)K_r\sigma_f}\right]\right\} \tag{49}$$

rather than this expression with $b=c=d=1$, but everything else is the same. For small values of σ_f and K_r, the angle δ changes little with variation of b, c, and d. In this respect, our BDPM model is robust.

It appears that the number of parameters in the analysis cannot be reduced beyond 3. This reinforces our belief that the BDPM system is a distinctive system that is well worth studying.

Our present interest is largely in the way the BDPM situation differs from the LTNE model for a regular porous medium. It now appears that the latter is the nongeneric case, one that requires an asymptotic analysis involving the matching of inner and outer solutions, occasioned by fact that the solid-phase temperature in a regular medium decays relatively slowly with distance normal to the boundary wall.

We conclude with some remarks about the status of our model, which is radically new and in some respects tentative. As far as we are aware, the only published works on the model are our papers [3–5,14]. In formulating this model, we aimed for the simplest possible model that would capture the main physical phenomena, such as velocity dispersion, in a BDPM. No attempt at derivation by volume averaging has yet been made, and to the best of our knowledge, no suitable experimental correlations for a BDPM are available. We hope that our work will stimulate relevant experimental and theoretical investigations. Our interphase momentum transfer parameter is currently a parameter to be determined by subsequent experiment. Brinkman effects can be treated by adding the usual Brinkman term, as in Refs. [3–5]. (These are necessary if information about wall friction is desired.) The effect of Forchheimer drag (and quadratic advective inertial terms) is a topic for further investigation.

Nomenclature

- c = specific heat at constant pressure
- d = characteristic length scale
- $\mathbf{G}$ = negative of the applied pressure gradient
- $\hat{g}$ = gravitational acceleration
- h = interphase heat transfer coefficient (incorporating the specific area)
- $\hat{h}$ = dimensionless interphase heat transfer parameter, $hd^2/\phi k_f$
- H = $\hat{h}/R$
- k = thermal conductivity
- K = permeability
- K_r = permeability ratio, K_p/K_f
- p^* = pressure
- R = Rayleigh number, $\rho_F g\hat{\beta}(T_w - T_\infty)K_f d/[\mu\phi k_f/(\rho c)_f]$
- T^* = temperature
- T_F^* = volume average temperature defined in Eq. (3)
- T_w = wall temperature
- T_∞ = ambient temperature
- u^* = x-component of velocity
- v^* = y-component of velocity
- $\mathbf{v}^*$ = filtration velocity, (u^*, v^*)
- x^* = vertical coordinate
- y^* = horizontal coordinate

Greek Symbols

- β = modified thermal capacity ratio, $(1-\phi)k_p(\rho c)_f/[\phi k_f(\rho c)_p]$
- $\hat{\beta}$ = volumetric thermal expansion coefficient of the fluid
- γ = modified thermal conductivity ratio, $\phi k_f/[(1-\phi)k_p]$
- Γ = parameter defined in Eq. (40)
- δ = parameter defined in Eq. (28b)
- ε = porosity within the p-phase
- ζ = coefficient for momentum transfer between the two phases
- η = boundary-layer parameter defined in Eq. (23)
- $\tilde{\eta}$ = modified boundary-layer parameter defined in Eq. (29b)
- θ = dimensionless temperature defined in Eq. (8)
- μ = fluid viscosity
- ξ = parameter defined in Eq. (30)
- ρ = density
- ρ_F = density of the fluid
- σ_f = f-phase momentum transfer parameter, $\zeta K_f/\mu$
- τ = $\phi/[\phi+(1-\phi)\varepsilon]$
- ϕ = volume fraction of the f-phase

Subscripts

- f = fracture phase (macropores)
- p = porous phase (micropores)

Superscript

- $*$ = dimensional variable

References

[1] Chen, Z. Q., Cheng, P., and Hsu, C. T., 2000, "A Theoretical and Experimental Study on Stagnant Thermal Conductivity of Bi-Dispersed Porous Media," Int. Commun. Heat Mass Transfer, **27**, pp. 601–610.

[2] Chen, Z. Q., Cheng, P., and Zhao, T. S., 2000, "An Experimental Study of Two Phase Flow and Boiling Heat Transfer in Bi-Disperse Porous Channels," Int. Commun. Heat Mass Transfer, **27**, pp. 293–302.

[3] Nield, D. A., and Kuznetsov, A. V., 2004, "Forced Convection in a Bi-Disperse Porous Medium Channel: A Conjugate Problem,"Int. J. Heat Mass Transfer, **47**, pp. 5375–5380.

[4] Nield, D. A., and Kuznetsov, A. V., 2005, "A Two-Velocity Two-Temperature Model for a Bi-Dispersed Porous Medium: Forced Convection in a Channel," Transp. Porous Media, **59**, pp. 325–339.

[5] Nield, D. A., and Kuznetsov, A. V., 2006, "The Onset of Convection in a Bidisperse Porous Medium," Int. J. Heat Mass Transfer, **49**, pp. 3068–3074.

[6] Nield, D. A., and Kuznetsov, A. V., 2005, "Heat Transfer in Bidisperse Porous Media," *Transport Phenomena in Porous Media III*, D. B. Ingham and I. Pop, eds., Elsevier, Oxford, Chap 2.

[7] Cheng, P., and Minkowycz, W. J., 1977, "Free Convection About a Vertical Plate Imbedded in a Porous Medium With Application to Heat Transfer From a Dyke," J. Geophys. Res., **82**, pp. 2040–2044.

[8] Rees, D. A. S., and Pop, I., 2000, "Vertical Free Convective Boundary-Layer Flow in a Porous Medium Using a Thermal Nonequilibrium Model," J. Porous Media, **3**, pp. 31–44.

[9] Mohamad, A. A., 2001, "Natural Convection From a Vertical Plate in a Saturated Porous Medium: Non-Equilibrium Theory," J. Porous Media, **4**, pp. 181–186.

[10] Rees, D. A. S., and Pop, I., 2002, "Comments on 'Natural Convection from a Vertical Plate in a Saturated Porous Medium: Non-Equilibrium Theory' by A. A. Mohamad," J. Porous Media, **5**, pp. 225–227.

[11] Haddad, O. M., Al-Nimr, M. A., and Al-Khateeb, A. N., 2004, "Validation of the Thermal Equilibrium Assumption in Natural Convection From a Vertical Plate Embedded in a Porous Medium: Non-Darcian Model," Int. J. Heat Mass Transfer, **74**, pp. 2037–2042.

[12] Haddad, O. M., Al-Nimr, M. A., and Al-Khateeb, A. N., 2004, "Validity of the Local Thermal Equilibrium Assumption in Natural Convection From a Vertical Plate Embedded in a Porous Medium," J. Porous Media, **8**, pp. 85–95.

[13] Nield, D. A., and Bejan, A., 2006, *Convection in Porous Media*, 3rd ed., Springer, New York.

[14] Nield, D. A., and Kuznetsov, A. V., 2008, "Natural Convection About a Vertical Plate Embedded in a Bidisperse Porous Medium," Int. J. Heat Mass Transfer, **51**, pp. 1658–1664.
[15] Rees, D. A. S., Bassom, A. P., and Siddheswar, P. G., 2008, "Local Thermal Non-Equilibrium Effects Arising From the Injection of a Hot Fluid Into a Porous Medium," J. Fluid Mech., **594**, pp. 379–398.
[16] Rees, D. A. S., and Bassom, A. P., 1991, "Some Exact Solutions for Free Convective Flows Over Heated Semi-Infinite Surfaces in Porous Media," Int. J. Heat Mass Transfer, **34**, pp. 1564–1567.
[17] Rees, D. A. S., 1993, "Nonlinear Wave Stability of Vertical Thermal Boundary Layer Flow in a Porous Medium," ZAMP, **44**, pp. 306–313.
[18] Rees, D. A. S., 2003, "Vertical Free Convective Boundary-Layer Flow in a Porous Medium Using a Thermal Nonequilibrium Model: Elliptical Effects," ZAMP, **54**, pp. 437–448.